Effect of Acoustic Noise on Optimal SynRM Design Regions

M. H. Mohammadi[1], T. Rahman[1], R. C. P. Silva[1], B. Wang[1], K. Chang[2] and D. A. Lowther[1]

[1] Department of Electrical and Computer Engineering, McGill University, Montreal, Canada
[2] Infolytica Corporation, Montreal, Canada

This paper investigates the design optimization of synchronous reluctance machines (SynRMs) in a multi-physics scenario. Using electromagnetic and structural finite element analysis (FEA) simulations, the average torque, torque ripple and loudness objectives are computed. In this digest, these three objectives are shown to be in conflict with each other, thereby resulting in a multi-objective problem. While the 33-slot 8-pole stator configuration is fixed, the SynRM's rotor is geometrically varied for different topologies, i.e. different numbers of flux barriers, for extracting optimal design regions which will be provided in the full paper.

***Index Terms*— AC machines, acoustic noise, design optimization, finite element analysis, torque.**

I. Introduction

Recently, the design of synchronous reluctance machines (SynRMs) has attracted significant research and development due to their low material cost, robustness and high torque-to-volume ratio for fixed speed applications. However, an important point of concern for SynRMs remains, since their rotor design is not a simple task. Selecting the right topology and geometry (i.e. barrier configuration and dimensions) has a major influence on a motor's performance, whether it is electromagnetic, acoustic or thermal.

In previous works [1], [2], [3], optimal design regions were extracted using the electromagnetic performance of two SynRM models: a 33-slot 8-pole and a 12-slot 4-pole. It was demonstrated in [2] and [3] that different topologies for a round-shaped barrier are interrelated based on the optimal values of average torque, T_{avg}, and torque ripple, T_{rip}. Nevertheless, these findings do not account for multi-physics aspects. For instance, would adding an extra objective, e.g. loudness, L_w, significantly impact the SynRM's optimization's outcome, such as the location and size of the optimal design region?

Therefore, this paper extends the design optimization of SynRMs by solving the multi-objective problem in (1) using three objectives, T_{avg}, T_{rip} and L_w. Both electromagnetic and structural finite element analysis (FEA) simulations are used for the objective computations of a 33-slot 8-pole SynRM as in [2] and [4]. Only the SynRM's rotor is geometrically varied for different topologies, i.e. different number of flux barriers, n_b, to extract optimal design regions which will be provided in the full paper. Here, $\boldsymbol{x}$ corresponds to a design variable vector and $\boldsymbol{\mathcal{F}_\Delta}$ demotes the feasibility triangle or design space.

$$\begin{aligned} \min_{\boldsymbol{x}} \quad & (-T_{avg}, T_{rip}, L_w). \\ \text{s.t.} \quad & \boldsymbol{x} \in \boldsymbol{\mathcal{F}_\Delta} \end{aligned} \tag{1}$$

II. Loudness Calculation and SynRM Rotor Geometry

Following [5], [6], the loudness of an electric machine is calculated using the amplitude of its stator vibrations. The stator is displaced by forces arising from the air gap pressure waves. The normal pressure wave component, P_n, at any angle, θ, along the air gap is calculated from the Maxwell stress tensor [5] and is given by (2). Here, F_n is the normal force on the stator tooth, L_{stk} is the stack length, w_s is the tooth width, B_n is the normal air gap flux density and μ_0 is the permeability of free space.

$$P_n(\theta) \approx \frac{F_n(\theta)}{w_s L_{stk}} = \frac{B_n^2(\theta)}{2\mu_0} \tag{2}$$

Note that tangential forces do not contribute significantly to the acoustic noise, since the teeth are constrained sideways. Due to the force's r^{th} harmonic on the m^{th} vibration mode, the stator's displacement, A_{mr}, is given by (3) as in [6]. Here, F_{n_r} is the r^{th} force amplitude, f_r is the r^{th} harmonic frequency, f_m is the m^{th} mode of natural vibration, M is the stator mass (core and winding) and ζ_m is the m^{th} harmonic of the damping factor.

$$A_{mr} = \frac{F_{n_r}/[(2\pi f_m)^2 M]}{\sqrt{[1-(f_m/f_r)^2]^2 + [2\zeta_m (f_m/f_r)]^2}} \tag{3}$$

The sound pressure level, SPL, on the surrounding air is computed using (4), where ρ_0 is the air density, c_0 is the speed of sound, and n_p is the number of poles. Then, the loudness value in dB, L_w, is calculated in (5) using SPL and $SPL_{ref} \approx 10^{-5}$ Pa.

$$SPL = 2\pi \rho_0 c_0 n_p \sum A_{mr} \tag{4}$$

$$L_w = 10 \log_{10}\left(SPL/SPL_{ref}\right) \tag{5}$$

Fig. 1 (a) illustrates an example of a single-barrier SynRM's cross-section with the labelled rotor variable widths: the flux carrier's, W_c, and the flux barrier's, W_b. The rotor barrier dimensions and the number of barriers, n_b, were varied to generate datasets of SynRM models for which T_{avg}, T_{rip} and L_w were calculated. For example, using a full factorial sampling for 90 designs across the single-barrier design space, (W_c, W_b), the response surfaces of T_{avg}, T_{rip} and L_w are then plotted in Fig. 1 (b), (c) and (d) respectively. It can be seen that L_w conflicts with both the T_{avg} and T_{rip} objectives. That is, the location of maximum T_{avg} in the (W_c, W_b) design space does not correspond to the minimum L_w location. Therefore, the suggestions proposed in [2] for restricting the design space do not hold when dealing with multi-physics problems including acoustic noise.

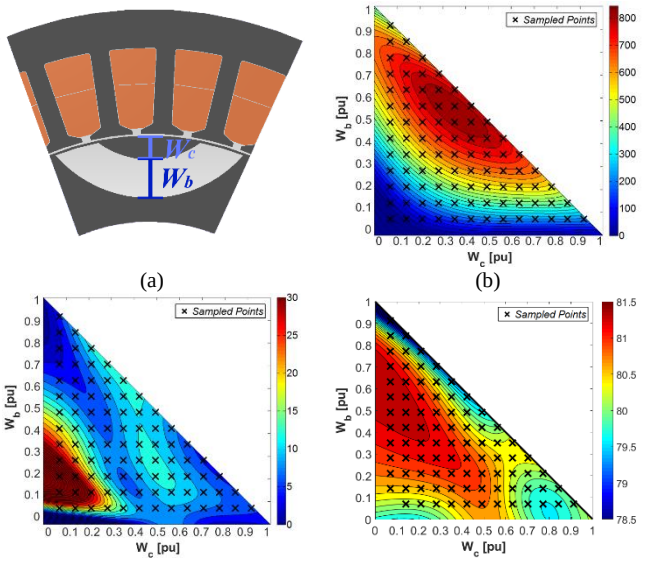

Fig. 1. (a) SynRM 1-barrier cross-section [2], (b) T_{avg} [Nm] response surface [2], (c) T_{rip} [%] response surface [2] (d) L_w [dB] response surface.

III. Preliminary Results and Future Work

Fig. 2 below shows all the 1-barrier SynRM solutions in the three objective spaces using 2D plots for simplicity. Note that the triangle point on the Pareto front of (L_w, T_{avg}) in Fig. 2 (a) does not correspond to an optimal T_{rip} value in Fig. 2 (b). A similar outcome is reached for the square point on the Pareto front of (T_{rip}, T_{avg}) in Fig. 2 (b) where the $L_w$value is high in Fig. 2 (a). Similar conflicts were observed for the 2-barrier and 3-barrier datasets of the SynRM example.

Furthermore, Fig. 3 below compares all the sampled values of the T_{avg}, T_{rip} and L_w objectives using boxplots. Note that as the number of barriers increases, all three objective values in (1) improve. That is, T_{avg} increases, T_{rip} decreases, and L_w decreases. Moreover, the range of objective values gets smaller for higher n_b tending toward optimal designs. This result also matches the design recommendations provided in the literature for SynRMs. Although L_w's range seems small at around 3 dB, this logarithmic value signifies a scaling factor of 2 between the smaller and larger SPL values.

To quantify the conflict level between the different objectives, the methodology described in [7] is implemented here. This becomes useful to quantitatively assess whether the objectives in a multi-objective problem need to be considered or not. In summary, a conflict level defines a relative measure between different objective pairs. For example, a 100% conflict means that improving one objective completely deteriorates the other. On the other hand, a 0% conflict signifies total harmony, where the improvement of one objective implies the same for its counterpart. Hence, a full factorial sampling of 90, 1366 and 5004 samples were performed for the 1, 2, and 3-barrier rotor topologies respectively while constraining all samples within $\boldsymbol{\mathcal{F}_\Delta}$. Then the conflict levels between each objective pair were computed; that is, (T_{avg}, T_{rip}), (T_{avg}, L_w) and (T_{rip}, L_w).

Table I below displays the conflict levels between all objective pairs for the three rotor topologies (i.e. 1, 2, 3-barrier). Note that for all combinations, the conflict levels are generally high and more than 50%. Only the (L_w, T_{rip}) pair's conflict decreases for higher n_b values. Nevertheless, these results indicate that the multi-objective problem in (1) is meaningful and it will be solved and analyzed in the paper's full version. This also means that the optimal design region using only (T_{avg}, T_{rip}) described in [2] and [3] will be impacted.

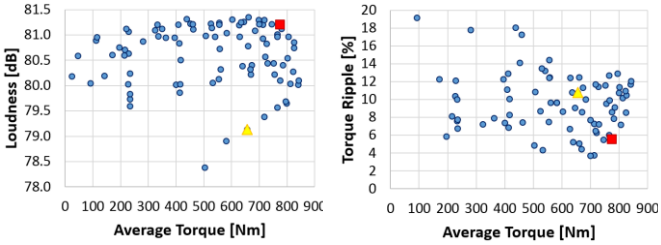

Fig. 2. Objective solutions for 1-barrier SynRM: (a) L_w, T_{avg}, (b) T_{rip}, T_{avg}.

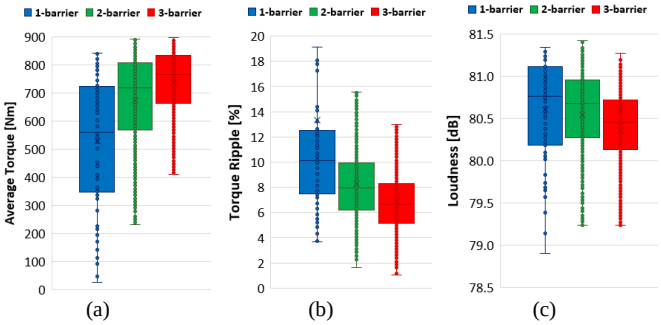

Fig. 3. Objective boxplots for different datasets: (a) T_{avg}, (b) T_{rip}, (c) L_w.

TABLE I
Conflict Level between Objective Pairs

n_b	T_{avg}, T_{rip}	T_{avg}, L_w	T_{rip}, L_w
1	52.4%	65.6%	67.8%
2	65.6%	62.8%	46.0%
3	68.7%	65.6%	34.2%

References

[1] G. Pellegrino, F. Cupertino and C. Gerada, "Automatic Design of Synchronous Reluctance Motors focusing on Barrier Shape Optimization," *IEEE Trans. Ind. Appl.,* vol. 51,no. 2, pp. 1465-1474, 2015.

[2] M. H. Mohammadi, T. Rahman, R. C. P. Silva, M. Li and D. A. Lowther, "A Computationally Efficient Algorithm for Rotor Design Optimization of Synchronous Reluctance Machines," *IEEE Trans. Magn.*, vol. 52, no. 3, pp. 1-4, Mar. 2016.

[3] M. H. Mohammadi, T. Rahman and D. A. Lowther, "Restricting the Design Space of Multiple-Barrier Rotors of Synchronous Reluctance Machines," in *the 17th Intl. IGTE Symposium on Numerical Field Calculation in Elect. Eng.*, Graz, Austria, Sep. 2016.

[4] J. F. Gieras, C. Wang, and J. C. Lai, *Noise of Polyphase Electric Motors*. CRC press, 2005.

[5] R. Islam and I. Husain, "Analytical model for predicting noise and vibration in permanent-magnet synchronous motors," *IEEE Trans. on Ind. Appl.,* vol. 46, no. 6, pp. 2346-2354, Dec. 2010.

[6] B. Wang, T. Rahman, K. Chang, M. H. Mohammadi, S. Sadagopan and D. A. Lowther, "Neural Network Based Surrogate Model for Predicting Noise in Synchronous Reluctance Motors," in *IEEE Conf. on Electromagn. Field Comp. (CEFC)*, Miami, FL, Nov. 2016.

[7] A. R. R. Freitas, P. J. Fleming and F. G. Guimarães, "A Non-Parametric Harmony-Based Objective Reduction Method for Many-Objective Optimization," in *IEEE Intl. Conf. on Systems, Man, and Cybernetics*, Manchester, Oct. 2013.